Electronic excitations of helium bilayers on a metal substrate

S. Kossler and P. Feulner*
Physik-Department E20, TU-München, 85747 Garching, Germany

J.-P. Gauyacq
Institut des Sciences Moléculaires d'Orsay, Unité mixte CNRS-Université Paris-Sud, UMR 8214, Bâtiment 351, 91405 ORSAY Cedex, France
(Received 21 August 2013; revised manuscript received 24 March 2014; published 9 April 2014)

Neutral one-hole, one-electron excitations converging to the He1*s* ionization limit of He bilayers on a metal surface are studied with linearly polarized synchrotron radiation and time-of-flight techniques. Comparing signals of emitted electrons, emitted He atoms in metastable excited states, and fluorescence photons as a function of photon energy and polarization with theoretical results, a detailed picture of the photoexcitation is obtained. We show that the width of the photoabsorption peaks is governed in an anisotropic way by the large zero point motion of the He atoms; broadening directly correlates with the shape of the electronic clouds of the absorbing states.

DOI: 10.1103/PhysRevB.89.165410 PACS number(s): 79.20.La, 73.20.−r, 67.25.bh, 79.60.Dp

I. INTRODUCTION

Condensation-induced modifications of electronic excitations are a key topic of condensed matter physics. For many semiconductors and insulators, outer shell to Rydberg excitations of the isolated atoms mutate into delocalized Wannier excitons. Polarization of the matrix reduces the excitons' binding energies compared to Rydberg states and spatially extends their wave functions. Particularly rare gas solids (RGSs) from Ne to Xe provided an appealing playground for the study of many aspects of Wannier excitons in matter, including energetics, trapping mechanisms and trapping dynamics, and the properties of surface states in regions of reduced symmetry [1–3].

In this context, condensed He is an extreme case that stands apart. The polarizability of condensed He is small [4], and due to the large negative electron affinity of condensed He of −1.3 eV [5], the repulsive interaction between electronically excited centers and the surrounding matrix is strong. Data on [He1*s*]*n*l excitations clearly rule out the assignment to Wannier exciton series valid for the heavier rare gases in the case of liquid and solid He [6–9], He bubbles in metals [10], and of He clusters and droplets [11–14]. k-dependence of the excitation energies has been observed only for high-density solids in pressure cells [9].

Instead, experiment [6–14] and theory [11,15–17] favor a different picture, depending on the principal quantum number n of the excited [He1*s*]*n*l state. Apart from extremely compressed He in bubbles [10], the wave functions of the $n = 2$ states are confined within the first shell of neighbors, whereas those of larger n extend over several shells. This has different effects: (i) a confinement-induced and therefore density-dependent blueshift and broadening, particularly of the [He1*s*]$n = 2$ derived lines in comparison to the Rydberg states of isolated atoms; (ii) the appearance of lines that are dipole forbidden for the isolated atom by mixing of states with different ℓ; and (iii) a pronounced sensitivity of excitation energies on the excitation site and its environment. [He1*s*]$n =$ 2 states are mainly affected by the first shell of neighbors and [He1*s*]$n > 2$ excitations also by the more extended surroundings [6–17]. At this point, the nature of condensed He as an archetype of a quantum substance [18] with very large zero point motion (ZPM) [19,20] comes into play. The confinement-induced blueshift of the excitation energies translates via this large ZPM amplitude into line broadening. Experiments with clusters and droplets of increasing density in the center demonstrate this nicely [11–13], in agreement with theory [11,15–17]. Cluster studies also indicate different behavior of surface and bulk excitations, as expected [11]. Opposed to crystals of the heavier RGSs that show well-ordered surface layers, and for which comprehensive data on surface excitons exist [1–3], the bulk-to-surface interface is less well defined for He clusters. Their density drops continuously over a rather thick boundary layer of ∼0.7 nm to zero [21]. This makes a clear discrimination of bulk and surface states and their density related energy changes difficult. Indirect conclusions are required, based, e.g., on comparison of fluorescence signals with different decay times, and on cluster size effects [11]. To the best of our knowledge, no attempts have been made to characterize interface states of He enclosed in pressure cells or in bubbles. In summary, a variety of effects contributes to the condensation shifts seen for [He]$n\ell$ states that are hard to disentangle unless the geometry of the investigated objects is simplified compared to previous experiments and investigated in a multiprobe experiment.

In this article, we report on such a study of a well-defined two-dimensional (2D) system, a He bilayer on top of a close-packed single-crystal surface. Such layers are perfectly reproducible and possess a similar density as solid He due to the Van der Waals attraction by the metal [22]. They are fully compatible with the requirements of a photoemission spectroscopy (PES) experiment in ultrahigh vacuum (UHV). The top He layer is sufficiently decoupled from the substrate to reveal He-specific excitation properties. The confinement of excited centers is well defined in all directions, i.e., no confinement toward the vacuum, and lateral and horizontal confinement by the neighboring atoms in the layer and underneath and by the substrate. This enables meaningful polarization experiments. Excitation with narrow bandwidth vertically or horizontally polarized synchrotron radiation (SR) and the detection of different probes (photo- and decay

*Corresponding author: feulner@tum.de

electrons, fluorescence photons, and desorbing metastable He* atoms) associated with theoretical calculations lead to a detailed picture of the energetics, electronic composition, and the decay routes of excited states in He bilayers on a metal surface. In particular, we are able to unveil the role of ZPM and its interplay with the shape of the excited orbitals.

II. EXPERIMENT

The data have been collected at the UE112-PGM and TGM-7 beamlines of the SR source BESSY-II, Berlin, with a time-of-flight (TOF) spectrometer utilizing the single bunch operation mode of this light source. Investigation of He layers physisorbed on metal surfaces is nontrivial, in particular under the conditions of a SR experiment. For bilayers, sample temperatures below 1.2 K and complete shielding of the black-body radiation from the 300 K environment is necessary to avoid rapid infrared (IR)-induced desorption [23]. A ^{4}He bath cryostat was built for this purpose. It was pumped by two root pumps (1000 m^3/h and 500 m^3/h) and a rotary piston pump (200 m^3/h) connected in series. The bath temperature of 0.9 K was measured with carbon resistors. The lifetime of one liquid He filling (250 ml) was at least 3 hours. The Ru(0001) crystal on which we prepared the He bilayers was attached to this cryostat by a monocrystalline W rod with very good heat conductivity at low temperature. A radiation shield cooled to 80 K surrounded the cryostat, the crystal mount, and the spectrometer. The SR entered this shield through a small aperture. The orientation of the **E** vector was either parallel to the surface (A_{xy} polarization) or tilted by 10° with respect to the surface normal (mainly A_z polarization; see [24] for more details of the experimental setup).

The Ru(0001) substrate was cleaned by sputtering with Ne^+, repeated heating to 1450 K in 10^{-7} mbar of O_2, and final flashing to 1570 K for 60 s [25]. Crystallographic order, including the absence of misorientation, was checked by low energy electron diffraction (LEED) and cleanliness by PES of core (C1*s*, O1*s*) and valence levels (He1*s* and substrate/contaminant levels). In particular, the shape and the position of the vacuum edge (see below), which depends on the work function of the sample, were sensitive to contaminations. Amounts of adsorbed water in the low percentage range of a monolayer caused a shift to lower energy as well as a broadening of the cut-off at the vacuum level. We designed the cryostat so that cooling of the sample from 1570 K to less than 1.2 K took less than 20 min to ensure perfect substrate cleanliness. After cleaning and cooling, He was dosed onto the crystal through a capillary integrated into the TOF spectrometer, and the coverage was checked by PES [24].

Before starting the He experiments, the surface quality of the Ru(0001) sample and particularly the absence of roughness has been checked by thermal desorption (TD) of Ar and Xe in a different UHV apparatus, in addition to the *in situ* surface checks by LEED mentioned above. This chamber was equipped with a mass spectrometer modified for high resolution TD studies (see [26] for details). Ar and Xe atoms bonded to defect states give rise to TD features different from the peaks related to the smooth surface [25]. The contribution of such defects sites to the total TD signal was below the 1% level for our crystal.

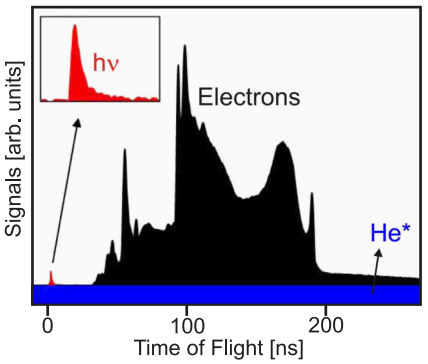

FIG. 1. (Color online) A TOF spectrum "as measured," showing contributions from fluorescence photons (red), desorbing metastable He* atoms (blue), and photoemission and decay electrons (black). See text for details.

We used a linear TOF spectrometer with a 25-cm-long drift tube. It was kept free from electric and magnetic fields by grids at both ends and a μ-metal shield. For data recording, the entrance grid of the spectrometer was positioned at a distance of 2 mm from the sample surface. The potential between sample and entrance grid was set in a way that the flight time of electrons from the vacuum level with vanishing initial kinetic energy was approximately 200 ns. A stack of two multichannel plates (MCPs) behind the exit grid of the drift tube served as detector. The output of the MCPs was amplified by 40 dB with a homemade amplifier of 5 GHz bandwidth and was further processed by a fast discriminator followed by two time-to-digital converters (TDCs) operated with 39-ps channel width [27]. A fast switch between the discriminator and the TDCs directed the even events to one of the TDCs and the odd events to the other. By this procedure, we reduced the minimum time interval for the recognition of pair events to less than 4 ns. BESSY's bunch marker with a 1.25 MHz repetition rate corresponding to an 800-ns interval between the light pulses during single bunch operation started data acquisition. Our timing accuracy of better than 100 ps [28] resulted typically in 2000 effective channels for spectra, as shown in Fig. 1.

Due to the linear geometry of our TOF spectrometer, electrons *as well as* photons and neutral He* atoms that propagate line of sight reach the detector of our device and are amplified by the MCPs, i.e., all of these probes are recorded simultaneously (see Fig. 1). Fluorescence photons traveling with speed of light appear *before* the onset of electron emission. From the exponential decay of the fluorescence signal, the lifetime of the excited state is obtained. Photodesorbed He* atoms, in contrast, are so slow that they do not reach the detector within 800 ns; their arrival is distributed over many of the single bunch cycles. They therefore show up as an $h\nu$-dependent background (Fig. 1, blue) under the fluorescence (Fig. 1, red) and the electron signals (Fig. 1, black). After untangling these contributions to the raw TOF signal by using their very different flight time distributions, the electron signal was converted from the TOF to the kinetic energy representation. In addition to the Jacobian transformation of the densities of states, we took the kinetic energy dependent acceptance angle of our spectrometer into account to obtain correct signal amplitudes [24,29]. We note that the TOF spectra

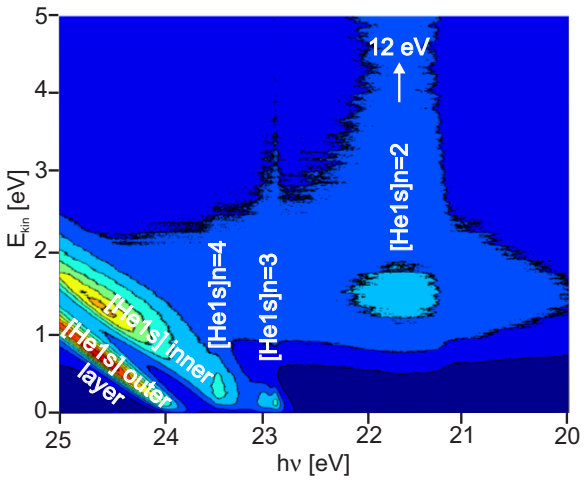

FIG. 2. (Color online) 2D electron spectrum from a He bilayer on Ru(0001) (A_z light, $E_{\rm kin}$ axis truncated). See text for details.

contain two intrinsic calibration marks for the kinetic energy scale of emitted electrons: The arrival time of stray light pulses corresponding to $E_{\rm kin} = \infty$, and the trailing edge of the electron distribution that is due to secondary electrons from the vacuum edge with vanishing $E_{\rm kin}$ (Fig. 1).

By combining $E_{\rm kin}$ distributions for closely spaced values of the photon energy, we obtained dense 2D electron spectra with the axes of kinetic and excitation energy, respectively (see Fig. 2 for an example). In these electron spectra, signatures of photoemission and neutral excitations are clearly discernible. In Fig. 2, [He1s] photoemission from the outer (ionization threshold at 23.83 eV) and the inner layer (threshold at 23.25 eV) appear as features with a slope of one. Neutral excitations in the outer layer are visible at constant photon energies around 21.6 eV, 22.9 eV, and 23.4 eV. Because of strong coupling to the metal, neutral excitations of the inner He layer are broad and weak and do not show up in this figure. Decay of the [He1s]$n = 2$ states stimulates electron emission with a maximum $E_{\rm kin}$ of 12 eV.

III. THEORY

A model theoretical study was performed on the He bilayer/metal system in order to precisely assign the He* states observed in the experimental spectra and to outline their links with free He* atoms. It parallels previous studies on Ne and Ar excitons [30–32]. It is a one-electron approach, based on wave packet propagation (WPP), i.e., one solves the time-dependent Schrödinger equation for the excited electron wave function $\Psi(\vec{r},t)$:

$$i\frac{d\Psi(\vec{r},t)}{dt} = (T + V_{e-\rm ion} + V_{e-\rm ion\ image} + V_{e-\rm He} + V_{e-\rm Surface} + V_{\rm Opt})\Psi(\vec{r},t), \quad (1)$$

where T is the electron kinetic energy. The various model potential terms above represent the electron interaction with the exciton ion core, the ion image, the He neighbors and the metal substrate. $V_{\rm Opt}$ is an absorbing potential at the edge of the computation box, set to enforce a pure outgoing boundary condition. The ion core potential $V_{e-\rm ion}$ is adapted from Ref. [33], and the e-He interaction potential has been adjusted from e-He scattering data following the procedure in Ref. [34]. The metal substrate is taken as a free-electron metal described with the local model potential $V_{e-\rm Surface}$ from Jennings *et al.* [35]. The electron wave packet is described in cylindrical coordinates centered on the He* with typically (450 × 64 × 1024) points in (ρ, φ, z) for 2 ML [36]. This choice of coordinates is well suited for the present system with a threefold rotational symmetry (sixfold for the monolayer) around the He*. It allows an accurate description of the He* and the first shells of He neighbors. Equation (1) is solved in the split operator approximation [37] with the initial condition $\Psi(\vec{r},t=0) = \Phi_0(\vec{r})$, where $\Phi_0(\vec{r})$ is typically chosen as an unperturbed atomic He* orbital. Analysis of the time-dependent wave packets $\Psi(\vec{r},t)$ yields the energies and lifetimes of the excited states in the system as well as their wave functions. In the present study, electron escape from the excited He* into the metal is an open channel; this results in a finite lifetime of the He* states, and the corresponding decay rate is obtained via the WPP calculations. This decay channel corresponds to the one-electron energy-conserving charge transfer process for the He* decay. It contributes to the broadening of the He* lines and is one of the key parameters for the discussion of He* survival probability in the desorption channel.

Additional calculations using the initial condition $\Psi(\vec{r},t = 0) = u = \Phi_{\rm Core}(\vec{r})$, where u is an electron coordinate and $\Phi_{\rm Core}(\vec{r})$ is the wave function of the core level of the $V_{e-\rm ion}$ potential, were also performed to get an estimate of the photoabsorption spectrum and its change with light polarization. Whereas the line positions and widths are accurate, this procedure only gives an approximate estimate of the peak heights in the absorption spectrum. Further details on the WPP procedure can be found in Refs. [30] and [38] and references therein.

The He atoms surrounding the He* exciton are arranged in a bilayer according to perfect fcc/hcp crystal positions. Only a finite cluster is considered, typically containing 60 He atoms with an interatomic distance equal to 6.75 atomic units. Such an approach assumes the He* excited states to be localized on the time scale of the electron dynamics. Actually it describes how an excited He* state is perturbed by a set of He neighbors and a metal surface, as described in the introduction. Additional calculations were performed with the He* atom displaced from its perfect crystal position, either along the normal to the surface or parallel to it, in order to probe the effect of ZPM on the absorption spectra. This only yields an estimate of the ZPM effect since only the He* is displaced.

IV. RESULTS AND DISCUSSION

As one of the main outputs of the present work, for each of the two light polarizations, Fig. 3 provides in parallel: the yield of desorbing neutral metastable He* atoms, the yield of fluorescence (FY) photons, and the partial electron yield (PEY) together with the theoretical photoabsorption spectrum. Within experimental scatter, the fluorescence lifetime coincides with the gas phase value of 0.55 ns for the $[1s]2p$ state [39]. The PEY signal was obtained by integrating the electron signal over the entire kinetic energy range covered by the decay electrons. The background from substrate and monolayer emission has been subtracted. Several peaks are clearly resolved between

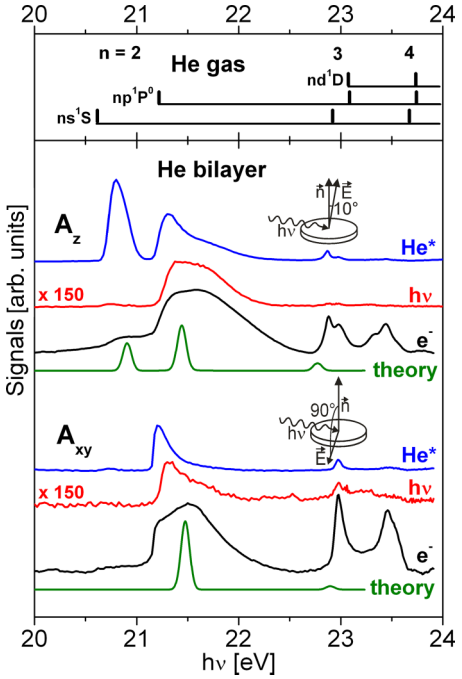

FIG. 3. (Color online) Yields of metastable He* atoms, fluorescence photons ($h\nu$), and electrons (e^-) from a He bilayer on Ru(0001) as a function of photon energy and polarization (see insets for the orientation of the **E** vector) compared to theoretical photoabsorption data convoluted with a 100-meV Gaussian. Compared to He gas (top, [40]), the bilayer excitation series is compressed.

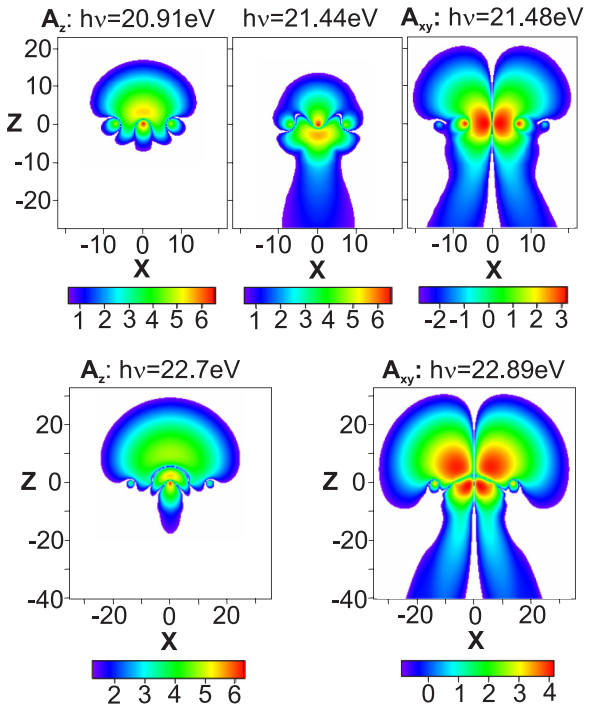

FIG. 4. (Color online) Cuts of the calculated electron density of the $n = 2$ (top) and $n = 3$ (bottom) Σ and Π states in the (X, Z) plane. Logarithmic scale according to the color bars. Origin of coordinates is on the He* center; Z ($\perp$ to the surface, $Z > 0$ in vacuum) and X ($\parallel$ to the surface, going through one of the first He neighbors) are in atomic units.

the onset of photoabsorption at 20.6 eV and the [1s] edge at 23.83 eV. For A_z light, which excites states of Σ symmetry with respect to the surface normal, we find the first absorption maximum at 20.8 eV, slightly above the $[1s]2s$ value of He gas at 20.62 eV [40]; it is strong in He*, weak in PEY, and nearly absent in FY. The second maximum is broad and centered at 21.55 eV (PEY), which is above the atomic $[1s]2p$ line at 21.22 eV [40]. It appears in all probe signals but with different shapes. At higher energies at 22.88 and 22.98 eV, we find two well-resolved maxima close to the atomic $[1s]3p$ line (23.09 eV [40]). At 23.45 eV, a fourth peak with a shoulder at 23.32 eV is seen, slightly below the atomic $[1s]4p$ transition at 23.74 eV [40]. These maxima at higher excitation energy are weak in the He* signal, and also in the FY traces (Fig. 3). In summary, we find for A_z light a set of two Σ states for each principal quantum number $n = 2$, 3, and 4. For A_{xy} light, which excites Π states with respect to the surface normal, the high-energy parts of these doublets persist (at 21.50, 22.98, and 23.46 eV in PEY), but the low energy parts are much weaker (20.75 eV) or completely absent [41].

Our calculations reproduce the experimental finding well, particularly for the $n = 2$ region. Here we find two Σ states, both with mixed s and p character but only one Π state with contributions from $2p$ but also from $3d$. For the larger principal quantum numbers, the calculation is less precise and the splitting of the Σ states is not reproduced. Figure 4 presents the electron density of the various quasistationary states in the system. The two lowest A_z states look very much like the two $n = 2$ s-p Stark hybrids of the linear Stark effect [42]; in particular, the lowest one is dominantly localized in vacuum. In contrast, the lowest A_{xy} state is much less perturbed (a $2p\pi$ state slightly mixed with $3d\pi$) and appears to be confined by the He neighbors in the same layer. The two highest states in Fig. 4 are considerably perturbed. They are both dominantly localized in vacuum and retain some $n = 3$ character, though they cannot be assigned to a single 3ℓ atomic state. In this case, confinement/repulsion by neighbors is so strong that the electronic cloud is repelled into vacuum.

The relative amplitudes of the maxima in the He*, FY, and PEY signals shed light on the decay routes of the different states. Detection of He* or fluorescence photons both require the following: (i) rapid desorption of the excited atom to avoid de-excitation via the first He layer with lower ionization limit or/and the substrate underneath [43], either by resonant charge [30] or near-field energy transfer [44]; and (ii) appropriate asymptotic behavior: $[1s]2s$ for the He* signal and $[1s]2p$ for radiative decay [45]. For a large PEY signal, on the contrary, coupling to the substrate is favorable. The density plots in Fig. 4 show that the latter requirement is fulfilled for the Π and the second Σ state of the $n = 2$ excitations. The first Σ state with strong $2s$ character extends mainly into the vacuum, pointing to slow de-excitation by electron transfer, in perfect agreement with the experiment. All plots show the confinement of the wave functions by the neighboring atoms [11,15–17] that creates the driving force toward desorption via the cavity desorption mechanism [46] (see Ref. [24] for a detailed analysis of the individual decay processes). We note, however, the surprising appearance of a small He* signal for the A_{xy} symmetry, which according to

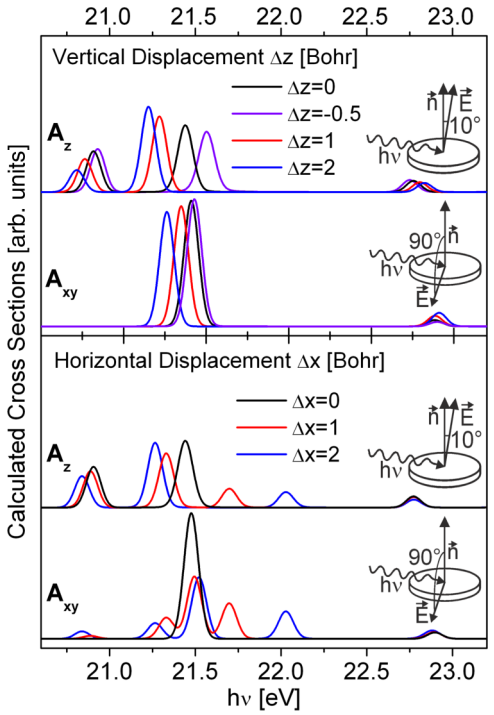

FIG. 5. (Color online) Calculated absorption spectra for A_z and A_{xy} light as a function of vertical (top, $\Delta Z > 0$ toward vacuum) and horizontal (bottom) displacement of the excited atom with respect to the fixed matrix (see text for details). Note that admixture of $2s$ character with He^* asymptotic by horizontal displacement (A_{xy} spectrum) prevails for the energy range below 21.5 eV (compare Fig. 3).

our calculations should not contain $2s$ character. We will show below that this is only true if ZPM is neglected.

The very large widths of the peaks in the various spectra are in agreement with results obtained previously [6–14]; they are attributed to the ZPM of the He atoms (see Fig. 5). We adopt a value obtained for solid He of $\langle z \rangle = 0.96\text{Å} = 1.81$ atomic units (for one dimension) [19], which is in line with calculations [20]. This value, which has been obtained for a bulk crystal, is certainly a lower limit for our samples with their free surfaces at larger temperature and at lower pressure. In Fig. 5, spectra calculated for a few distinct displacement values ΔZ and ΔX are shown. Because the electronic transition is instantaneous (vertical), it randomly probes all displacement values due to ZPM. The experiment therefore averages over all spectral shapes related to the continuum of ΔX and ΔZ values within the amplitude of ZPM, resulting in the peak broadening seen in Fig. 3.

For *vertical* displacements toward the vacuum ($\Delta Z > 0$), the wave function confinement is decreased, and the excitation energies of Σ and Π states are redshifted toward the gas phase values (Fig. 5). We note that for the higher quantum numbers this shift is smaller ($n = 3$ manifold) or even in the opposite direction. Actually, the energy shift due to ΔZ is directly correlated with the amount of electronic density pointing toward the substrate (Figs. 4 and 5), confirming the importance of confinement. Concurrently, the mixing of $2s$ and $2p$ and $2p$ and $3d$ for the Σ and Π states is reduced for $\Delta Z > 0$, and the excitation cross sections are changed accordingly: The first Σ peak decreases (toward the vanishing intensity of the dipole-forbidden $[1s]2s$ state), the second Σ maximum increases (toward the dipole-allowed $[1s]2p$ state), and the Π state decreases because the admixture of the d component vanishes. Movement toward the substrate causes changes in the opposite directions.

ZPM *parallel* to the surface has an even stronger effect, stressing the non-isotropic impact of ZPM. The states that are dominantly localized in vacuum (Fig. 4) are moderately influenced by a ΔX displacement in contrast to the Π state at 21.44 eV, which is confined between two neighbors along the X direction. The ΔX displacement breaks the crystal symmetry and splits the Π state at 21.44 eV into two states, symmetric and antisymmetric with respect to the XZ plane. The symmetric part mixes with the Σ states that are also symmetric with respect to this plane. This results in three or four different $[1s]n = 2$ states for A_z or A_{xy} light, respectively (Fig. 5), a substantial peak broadening and the appearance of a low lying peak for A_{xy} light (Fig. 5) that explains the observation of the He^* signal also for this polarization (see Fig. 3). We note, however, that $2p$ to $2s$ transitions during the desorption process, either substrate mediated [44] or via an excimer potential energy surface [47,48], could also produce a desorbing metastable He^*. The widths of the $n = 2$ Σ and Π maxima estimated for a lateral ZPM amplitude of 1.81 atomic units are around 750 and 550 meV, respectively, i.e., in good agreement with the experimental PEY values of 730 and 580 meV. The broadening due to the vertical ΔZ displacement is smaller by a factor of 2 (Fig. 5).

V. SUMMARY

We have shown that polarization-resolved excitation measurements, in combination with model calculations, reveal a very detailed picture of the electronic excitations in the surface layer of a 2D He bilayer system on a metal substrate. Neutral excited states with the principal quantum numbers two, three, and four were evidenced. For each principal quantum number, contributions with different orbital momenta are strongly mixed; the compositions depend on the symmetry of the excited states and the lateral and vertical displacements at the instant of excitation that partly break this symmetry. These displacements are governed by the ZPM, i.e., the quantum character of the condensed He. The possibility of changing the light polarization with respect to the surface normal and the simultaneous recording of different probes brought significant information on both the decay routes and the asymptotic character of the various individual He^* states in the system. These two features have been essential for the successful assignment and disentangling of the various effects seen in the excitation spectrum of this prototypical system.

ACKNOWLEDGMENTS

We thank R. Schneider, N. Armbrust, and the staff of BESSY for help during the experiments. SK and PF acknowledge support from J.V. Barth, the Deutsche Forschungsgemeinschaft (Projects Fe 286/2-1 and the Munich-Centre for Advanced Photonics MAP B.1.4.) and by the Helmholtz-Zentrum-Berlin, and helpful comments from D. Menzel. Computations were partly performed with the GMPCS high performance computer facilities of the LUMAT Fédération de laboratoires d'Orsay.

[1] N. Schwentner, E.-E. Koch, and J. Jortner, *Electronic Excitations in Condensed Rare Gas Solids*, Springer Tracts in Modern Physics 107 (Springer, Berlin, 1985), and references therein.

[2] G. Zimmerer, *Excited State Spectroscopy in Solids* (North Holland, Amsterdam, 1987), p. 37, and references therein.

[3] B. Kassühlke, R. Romberg, P. Averkamp, and P. Feulner, J. Low. Temp. Phys. **111**, 723 (1998).

[4] ε values of 1.056 and 1.042 are reported for condensed ^{4}He and ^{3}He, respectively: Y. Monarkha and K. Kono, *Two-Dimensional Coulomb Liquids and Solids*, Springer Series in Solid-State Sciences 142 (Springer, Berlin, 2004).

[5] T. Sommer, Phys. Rev. Lett. **12**, 271 (1964).

[6] C. M. Surko, G. J. Dick, F. Reif, and W. C. Walker, Phys. Rev. Lett. **23**, 842 (1969).

[7] D. A. Arms, T. J. Graber, A. T. Macrander, R. O. Simmons, M. Schwoerer-Böhning, and Y. Zang, Phys. Rev. B **71**, 233107 (2005).

[8] N. Schell, R. O. Simmons, A. Kaprolat, W. Schülke, and E. Burkel, Phys. Rev. Lett. **74**, 2535 (1995).

[9] D. A. Arms, R. O. Simmons, M. Schwoerer-Böhning, A. T. Macrander, and T. J. Graber, Phys. Rev. Lett. **87**, 156402 (2001).

[10] C. A. Walsh, J. Yuan, and L. M. Brown, Philos. Mag. A **80**, 1507 (2000), and references therein.

[11] K. v. Haeften, T. Laarmann, H. Wabnitz, T. Möller, and K. Fink, J. Phys. Chem. A **115**, 7316 (2011), and references therein.

[12] R. Fröchtenicht, U. Henne, J. P. Toennies, A. Ding, M. Fieber-Erdmann, and T. Drewello, J. Chem. Phys. **104**, 2548 (1996).

[13] K. v. Haeften, T. Laarmann, H. Wabnitz, and T. Möller, J. Phys. B **38**, S373 (2005); T. Möller, A. R. B. De Castro, K. v. Haeften, A. Kolmakov, T. Laarmann, O. Löfken, C. Nowak, F. Picucci, M. Riedler, C. Rienecker, A. Wark, and M. Wolff, J. Electron Spectrosc. Rel. Phen. **101-103**, 185 (1999); M. Joppien, R. Müller, and T. Möller, Z. Phys. D **26**, 175 (1993); M. Joppien, R. Karnbach, and T. Möller, Phys. Rev. Lett. **71**, 2654 (1993).

[14] See the excitation spectra in O. Bünermann, O. Kornilov, D. J. Haxton, S. R. Leone, D. M. Neumark, and O. Gessner, J. Chem. Phys. **137**, 214302 (2012); O. Bünermann, O. Kornilov, S. R. Leone, D. M. Neumark, and O. Gessner, IEEE J. Sel. Top. Quantum Electron. **18**, 308 (2012).

[15] K. v. Haeften and K. Fink, Eur. Phys. J. D **43**, 121 (2007).

[16] K. D. Glosser and M. Head-Gordon, J. Phys. Chem. A **114**, 8023 (2010).

[17] N. C. Pyper, C. W. Essex, and C. T. Whelan, Philos. Mag. B **81**, 91 (2001), and references therein.

[18] See, e. g., N. R. Werthamer, Am. J. Phys. **37**, 763 (1969).

[19] C. A. Burns and E. D. Isaacs, Phys. Rev. B **55**, 5767 (1997).

[20] E. W. Draeger and D. M. Ceperley, Phys. Rev. B **61**, 12094 (2000).

[21] J. Harms, J. P. Toennies, M. Barranco, and M. Pi, Phys. Rev. B **63**, 184513 (2001); A similar effect is reported for He multilayer films: K. Penanen, M. Fukuto, R. K. Heilmann, I. F. Silvera, and P. S. Pershan, *ibid.* **62**, 9621 (2000).

[22] See, e.g., E. Zaremba and W. Kohn, Phys. Rev. B **13**, 2270 (1976); **15**, 1769 (1977).

[23] T. Niedermayer, H. Schlichting, D. Menzel, S. H. Payne, and H. J. Kreuzer, Phys. Rev. B **71**, 045427 (2005).

[24] S. Kossler, Ph.D. dissertation, Technische Universität München, 2011.

[25] See e.g., H. Schlichting and D. Menzel, Surf. Sci. **272**, 27 (1992).

[26] H. Schlichting and D. Menzel, Surf. Sci. **285**, 209 (1993).

[27] We used an ORTEC 9307 pico-timing discriminator and two ORTEC 9308 picosecond time analyzers. The fast switch was realized in emitter coupled logic with sub-ns switching time and negligible jitter.

[28] The timing uncertainty is due to the duration of the light pulse and the jitter of the bunch marker (typically 70 ps for both, slightly depending on the filling of the storage ring), the walk of the discriminator (<40 ps), and the jitter of the TDCs [<25 ps, all values are full width at half maximum (FWHM)]. Assuming Gaussian shapes and statistically independent contributions, we obtain a scatter of $\leq$85 ps FWHM.

[29] P. Feulner, P. Averkamp, and B. Kassühlke, Appl. Phys. A **67**, 657 (1998).

[30] J. P. Gauyacq and A. G. Borisov, Phys. Rev. B **69**, 235408 (2004).

[31] J. P. Gauyacq, Phys. Rev. B **71**, 115433 (2005).

[32] J. P. Gauyacq and A. K. Kazansky, Chem. Phys. **327**, 300 (2006).

[33] M. Aymar and M. Crance, J. Phys. B **13**, 2527 (1980).

[34] P. Valiron, R. Gayer, R. McCarroll, F. Masnou-Seeuws, and M. Philippe, J. Phys. B **12**, 53 (1979).

[35] P. J. Jennings, R. O. Jones, and M. Weinert, Phys. Rev. B **37**, 6113 (1988).

[36] Cylindrical coordinates have been used because of technical reason; their use does not imply cylindrical symmetry of the system under investigation.

[37] M. D. Fleit and J. A. Fleck, J. Chem. Phys. **78**, 301 (1983).

[38] A. G. Borisov, A. K. Kazansky, and J. P. Gauyacq, Phys. Rev. B **59**, 10935 (1999).

[39] A. A. Radzig and B. M. Smirnov, *Reference Data on Atoms, Molecules and Ions* (Springer, Berlin, 1985).

[40] S. Bashkin and J. O. Stoner Jr., *Atomic Energy Levels and Grotian Diagrams*, (North Holland, Amsterdam, 1975) Vol. 1.

[41] We note that contributions of double excitations of He can be excluded. Such excitations would require photon energies of 58 eV and more for isolated He atoms [see, e.g., Xiao-Jing Liu *et al.*, Phys. Rev. Lett. **91**, 193201 (2003)] as well as for our He bilayer system on metal surfaces (S. Kossler, diploma thesis, TU-München, 2007; S. Schaper, bachelor thesis, TU-München, 2013), i.e., well beyond the energy range investigated here.

[42] See, e.g., L. D. Landau and E. M. Lifshitz, *Quantum Mechanics* (Pergamon Press, Oxford, 1965) Chapter 10, paragraph 77; A. G. Borisov, R. Zimny, D. Teillet-Billy, and J. P. Gauyacq, Phys. Rev. A **53**, 2457 (1996).

[43] F. M. Penning, Naturwissenschaften **15**, 818 (1927).

[44] R. R. Chance, A. Prock, and R. Silbey, J. Chem. Phys. **62**, 2245 (1975).

[45] We note that deexcitation of the He* by near field energy transfer creates a He atom in the electronic ground state that would be invisible in our experiment even if desorbed. De-excitation by resonant charge transfer to the metal substrate creates an intermediate He^+ ion that is attracted to the surface by image forces. Its neutralization by an interatomic Auger process results in a ground state atom, as for the scenario above. Electronically

stimulated desorption of He^+ is energetically excluded for photon energies below 24.6 eV, i.e., the first ionization potential of isolated He.

[46] See, e.g., F. Coletti, J. M. Debever, and G. Zimmerer, J. Phys. Lett. **45**, L467 (1984); Desorption of He^* and He_2^* was also observed for clusters and droplets [11–14].

[47] C. C. Wang, O. Kornilov, O. Gessner, J. H. Kim, D. S. Peterka, and D. M. Neumark, J. Phys. Chem. A **112**, 9356 (2008), and references therein.

[48] M. L. Ginter and R. Battino, J. Chem. Phys. **52**, 4469 (1970); J. P. Gauyacq, J. Phys. B **9**, 2289 (1976).